EFDA–JET–CP(12)02/27

A. Huber, S. Brezinsek, M. Groth, P.C. de Vries, V. Riccardo, G. van Rooij, G. Sergienko, G. Arnoux, A. Boboc, P. Bilkova, G. Calabro, M. Clever, J.W. Coenen, M.N.A Beurskens, T. Eich, S. Jachmich, M. Lehnen, E. Lerche, S. Marsen, G.F. Matthews, K. McCormick, A.G. Meigs, Ph. Mertens, V. Philipps, U Samm, M. Stamp, M. Wischmeier, S. Wiesen and JET EFDA contributors

Impact of the ITER-Like Wall on Divertor Detachment and on the Density Limit in the JET Tokamak

Impact of the ITER-Like Wall on Divertor Detachment and on the Density Limit in the JET Tokamak

A. Huber[1], S. Brezinsek[1], M. Groth[2], P.C. de Vries[2], V. Riccardo[2], G. van Rooij[3], G. Sergienko[1], G. Arnoux[2], A. Boboc[2], P. Bilkova[4], G. Calabro[5], M. Clever[1], J.W. Coenen[1], M.N.A Beurskens[2], T. Eich[6], S. Jachmich[7], M. Lehnen[1], E. Lerche[2], S. Marsen[8], G.F. Matthews[2], K. McCormick[6], A.G. Meigs[2], Ph. Mertens[1], V. Philipps[1], U Samm[1], M. Stamp[2], M. Wischmeier[6], S. Wiesen[1]
and JET EFDA contributors*

JET-EFDA, Culham Science Centre, OX14 3DB, Abingdon, UK

[1]*Institute of Energy and Climate Research – Plasma Physics, Forschungszentrum Jülich, Association EURATOM-FZJ, D-52425 Jülich, Germany*
[2]*EURATOM-CCFE Fusion Association, Culham Science Centre, OX14 3DB, Abingdon, OXON, UK*
[3]*FOM-Institute DIFFER, EURATOM Association, Nieuwegein, Netherlands*
[4]*Institute of Plasma Physics, Academy of Sciences of the Czech Republic, Prague, Czech Republic*
[5]*Associazione Euratom-ENEA, Via Enrico Ferri 46, I-0044 Frascati, Italy*
[6]*Max-Planck-Institut für Plasmaphysik, EURATOM Association, D-85748 Garching, Germany*
[7]*Association 'EURATOM-Belgian state', Ecole Royale Militaire, B-1000 Brussels, Belgium*
[8]*Max-Planck-Institut für Plasmaphysik, EURATOM Association, D-17491 Greifswald, Germany*
** See annex of F. Romanelli et al, "Overview of JET Results", (23rd IAEA Fusion Energy Conference, Daejon, Republic of Korea (2010)).*

Preprint of Paper to be submitted for publication in Proceedings of the
20th International Conference on Plasma Surface Interactions , Eurogress, Aachen, Germany
21st May 2012 - 25th May 2012

ABSTRACT

L-mode and H-mode density limit experiments with the ITER-Like Wall (ILW) have been investigated in the recent experimental campaign and compared with experiments in the JET carbon material configuration. The density limit is up to 40% higher in the Be/W- than in the C-machine. This is linked to the higher radiation fraction and correspondingly to earlier divertor detachment in the C- configuration. In the ILW configuration, the discharge demonstrates a stable operation with a completely detached outer divertor or even with stable X-point MARFE giving an opportunity for the realization of a feedback control for stabilization of the operation domain under fully detached divertor conditions.

The H-L transition constitutes an effective undisruptive density limit for an H-mode plasma. Detachment itself does not trigger the H-L back transition, hence does not present a limit on plasma density. The H mode studies show that before an H mode quenches into an L mode the maximum achievable density is practically independent of the heating power.

1. INTRODUCTION

Tokamak operation at high density with a detached divertor is a key element of the current ITER baseline design [1]. Cold or detached divertor operation is mandatory to reduce the heat loads on Plasma-Facing Components (PFCs), in particular on the divertor target plates, to an acceptable level and to reduce the tungsten (W) sputtering [2]. In preparation for ITER, JET has been upgraded with a new ITER-Like wall (ILW) [3], whereby the main plasma-facing components, previously made of carbon, have been replaced by Be in the main chamber and W in the divertor. The installation of the ITER-like wall on JET gives an opportunity to study tokamak operation with an ITER-relevant mix of wall materials at densities close to the Greenwald limit and to compare it to the operation with the previous carbon-dominated first wall. Dedicated L-mode and H-mode density limit experiments have been performed during JET campaigns with the ITER-like wall and compared with experiments in the Carbon wall configuration which are operated under similar experimental conditions. The results of these experiments are summarized and discussed.

2. L-MODE DENSITY LIMIT EXPERIMENT IN THE JET TOKAMAK WITH THE ITER-LIKE WALL

2.1. EXPERIMENT

L-mode density limit experiments with the ILW have been performed at $B_T = 2.4T$, $I_p = 1.7MA$ in ohmic discharges and in discharges with an additional NBI-power of 1.0-4.0MW in low- and high-triangularity magnetic equilibria similar to those used in the all-carbon machine experiments. Figure 1 shows the time evolution of a typical L-mode density limit discharge in JET with the tungsten divertor. The plasma density was raised steadily to the density limit by gas fuelling into the inner leg of the divertor at constant input power. The integral ion flux to the outer divertor, measured by an array of Langmuir Probes (LP), initially increases whereas the flux to the inner divertor remains

at a constant level. This indicates that the inner divertor is partially detached from the beginning. At 21s, the D_γ emission in the inner divertor reaches its maximal value and the integral ion flux to the inner divertor begins to fall as the density increases; it reaches a very low value around 22s. The neutral pressure in the divertor chamber (not shown) continues to increase, though. This is the signature of plasma detachment [4], which is characterised by a substantial drop both in particle and energy fluxes to the target plates, as well as in the plasma pressure along the magnetic field lines. The ion flux to the outer divertor saturates around 21.5s and begins to decrease indicating the roll-over into detachment in the outer divertor leg. With continuous deuterium puffing, it continues to drop until a high density, low temperature plasma forms inside the separatrix near the X-point. This is the so-called X-point MARFE (XPM) which leads to a 'density limit' disruption. The general behaviour of the detachment is independent of whether a C or Be/W wall were used. The detailed analysis of the divertor detachment in a carbon environment with magnetic field configurations similar to those discussed in this paper can be found in [5].

2.2 CHARACTERIZATION OF DIVERTOR DETACHMENT AND ROLE OF DETACHMENT IN L-MODE DENSITY LIMIT

Volume recombination in hydrogenic plasmas plays an important role in plasma detachment from the target plates of diverted discharges [4]. Experimental evidence of recombination has been obtained in JET from the increase in the ratio of the intensities of the Balmer series lines of excited hydrogen atoms, D_γ/D_α and D_β/D_α [6,7] or in the increase of the recombination continuum at series limit. For characterisation of the plasma detachment processes, it is very important to determine the source of impurities and of their radiation distribution in front of all plasma-facing components as well as to determine which regions of the divertor are affected by recombination. The new endoscope [8], having an improved spatial resolution (≤3mm in the object plane) over previous designs and delivering images of high quality, gives a unique opportunity for monitoring the impurity radiation as well as the changes in the recombination region by simultaneous imaging of D_α, D_β, D_γ emission from the divertor with CCD cameras with the same Field of View. The recorded images are inverted by a singular value decomposition method [9,10,11] to provide local emissivities. The two divertor spectroscopy systems for the visible and near-UV spectral range viewing the divertor region over 21 lines of sight are used for cross-checking/calibration and for comparison with the reconstructed 2D distributions of the line radiation [12].

In figure 2 the time traces of the local ion currents in the outer divertor region are shown for the L-mode density limit shown in figure 1. The strike points for this pulse are on the vertical JET divertor tiles. A reduction in ion current at the outer strike point (IsOSP) is observed at 21.3s. Nonetheless, the outer SOL currents continue to increase until 21.4s and 21.6s for Langmuir Probes (LPs) located on flux surfaces, which map to 0.45, 0.65 and 1.62cm from the separatrix at the outer midplane. Detachment thus occurs in a similar way as in the C-machine [5,13], first at the separatrix and it then propagates deeper into the SOL with time. At 22.0s, the outer divertor completely detaches and,

in contrast to the C-wall machine, it does not immediately trigger the X-Point MARFE formation. The line averaged density continues to increase even with a completely detached outer divertor until the X-Point MARFE formation leads to a 'density limit' disruption.

Furthermore, figure 2 shows snapshots of the Dγ-emissions (top) and Dγ/Dα ratios (bottom) in the divertor region during the pulse time evolution:

- Time 21s: In this early phase of the discharge, the maximum of the hydrogen radiation is located near the target plates at the position of the strike zone but with significantly more radiation from the inner leg than from the outer. The electron temperature near the inner and outer strike points is about 2eV and 5eV, respectively.
- Time 21.4s: The Dγ-emission rapidly increases in the outer divertor. The ion flux to the inner divertor decreases, which indicates the start of the detachment. The D_γ/D_α-ratio increases slightly in the vicinity of the outer strike point.
- Time 21.7s: Outer Divertor: the Outer Strike Point is detached. The detachment propagates into the SOL. The D_γ/D_α-ratio increases strongly in the SOL.
- Time 22.32s: Strong recombination in the deep SOL. The radiation pattern moves inside the LCFS.
- Time 22.41s: Formation of the X-point MARFE. It lives about 0.2s and proceeds with movement towards the inner wall, which leads to a density-limit disruption.

The comparison of the recorded emissions between CCD cameras and spectroscopy systems shows good correlation in the emissions behaviour between two independent systems.

2.3 COMPARISON OF THE DETACHMENT BEHAVIOUR IN C- AND FULLY METALLIC MACHINE

In figure 3 the ILW density limit discharge (JET-ILW) discussed above is directly compared with an identical case performed with the Carbon wall (JET-CFC). Both plasmas (1.7MA/2.4T) were heated with ≈2MW NBI. The onset of the X-point MARFE, which is a precursor to the ultimate density limit, occurred at higher densities (+40%) when the experiment was performed in the fully metallic machine. The general behaviour of the ion saturation current in the inner divertor is independent of whether C or Be/W wall were used. In both cases, the inner divertor is partially detached from the beginning. On the other hand, the ion flux to the outer divertor (I_s^{outer}) behaves differently. Shortly after the outer divertor rollover to detachment in the JET-CFC, the ion flux to the outer divertor drops dramatically: a MARFE forms, which leads on a short time scale to a 'density limit' disruption. Opposite to the C wall, the ion flux to the outer divertor in the machine with ILW saturates and begins slowly and monotonously to decrease with continuous deuterium puffing. During this continuous drop, the density still rises and the discharge demonstrates a stable phase with a completely detached outer divertor. In the ILW configuration, the lifetime of the completely detached outer divertor, as well as the X-point MARFE, is much longer than in the carbon environment, giving more flexibility for the realization of a feedback control for stabilization of the

operation domain under full divertor detachment. In contrast to the JET-ILW, the feedback control of the completely detached divertor performed in the JET-CFC [5] demonstrates the high level of the complexities and difficulties. In both experiments, the total radiated power is always increasing during the density increase. Interestingly, the radiation level and the corresponding power flux across the separatrix ($q_{perp} = (P_{heat}-P_{rad})/S$, where S is the plasma surface) is approximately the same at the moment of X-point MARFE formation despite the higher density limit in the case of the ILW.

At the same line averaged ne, the radiation fraction is higher in JET-CFC than in JET-ILW as shown in Fig.4. More radiation leads to a reduction of q_{perp} as well as of power fluxes to the divertor plates [14] and consequently to earlier detachment, at the strike point and also in the SOL, for the machine with C-wall. At the same time, the gas pressure is larger for the Be/W wall environment. We have here two competing processes leading to earlier detachment: more radiation and more gas pressure. The radiation level is the dominant process responsible for the earlier detachment : it leads to earlier detachment and, correspondingly, to a lower density limit in the C-machine. Comparison experiments with JET-CFC and JET-ILW demonstrate a strong reduction of the C content by at least a factor 10 [15] and associated modelling [14] reveals the contribution of the different partners to the radiation.

The obvious difference between ILW and C-wall is the fact that with density rise, T_e in the divertor drops leading to significant reduction of W sputtering [2]. Beryllium is a much weaker radiator than C and a significant fraction of the radiation in JET-ILW is caused by deuterium [14]. In contrast to the ILW case, the carbon machine still displays significant radiation from C, though complete absence of chemical and physical sputtering at the strike point [5]. It can be assumed that during the detachment the production of the hydrocarbons is not localised at the strike point and could take place across the entire divertor wall surface due to chemical erosion caused by thermal and also energetic neutrals (generated by charge-exchange) [13].These effects lead to lowering the radiation in JET-ILW and to stable operation with the completely detached divertor or even with a stable X-point MARFE.

Since the cause for development of the MARFE is the cooling instability in the plasma edge, we would expect an increase of the critical density for the MARFE onset by application of a strong auxiliary heating. To analyse this power dependence, the neutral beam auxiliary heating power was varied from 1.0 MW to 4.0 MW in the plasma discharges with $I_p = 1.7$MA and $B_T = 2.4$T. Figure 5 shows the measured line-average density at MARFE onset as a function of total heating power obtained in the JET experiments with C-and Be/W walls. The onset of an X-point MARFE appears at about 20% larger density for pulses in the full metal machine than for the C-based machine over the entire range of the observed heating powers. Additionally, Fig.5 shows the result for pulses with reversed field direction (ion ∇B drift direction away from the X-point). The target power asymmetries, which are probably a result of unequal power sharing between the targets due to classical drift effects [16], are smaller in the reversed field configuration. The outer divertor in the reversed field discharge is colder than in forward field operation and correspondingly detaches

earlier, what leads to a ~15% lower density limit. Additionally, an increase of total radiation fraction in the case with reversed field configuration has been observed. A moderate increase of the density limit with $P_{heat} = P_{NB} + P_{Ohm}$ was observed for both JET experiments with C-and Be/W walls ($<n_e>^{cr} \sim P_{heat}^{0.4}$).

2.4 L-MODE DENSITY EXPERIMENT WITH THE ILW IN A HIGH-TRIANGULARITY CONFIGURATION

While the density limit in L-mode JET plasmas with C-wall is generally disruptive, the extended operation range with ILW in high triangularity configuration can lead to prompt transition to a mode with a stable "completely detached divertor" or even with the stable X-point MARFE and a disruption is not inevitable. Figure 6 shows the time traces of the line integrated electron densities in the core and at the edge of two L-mode discharges ($I_p = 1.7$MA, $B_T = 2.4$T) in JET with high triangularity equilibrium configurations at 2MW and 4MW auxiliary heating powers. The plasma density was raised steadily by gas fuelling to the density at which the transition occurs, presumably caused by an MHD instability, to the mode with a stable X-point MARFE. This density represents the density limit for the L-mode plasmas with such configuration. The density limit was found to rise when the input power increases. Also the time window of the mode with stable X-point MARFE increases with the input power: from 05.s for $P_{NBI} = 2$MW to 1.0s for $P_{NBI} = 4$MW. Fig.6 (top) shows the clear appearance of Be II-emission inside the Last Closed Flux Surface (LCFS) during this stable mode. With gas fuelling the density peaking decreases towards complete flatness and shortly before the transition a hollow density profile ($n_e^{ped} > n_e^{core}$) forms, with H-mode like ne pedestal, as shown in the fig.6. MHD instability leads to an abrupt drop of the pedestal density triggering the transition to a mode with the stable "completely detached divertor" and with the stable X-point MARFE. To reach the density limit in the full metal machine, essentially larger puffing rates than for the C-based machine are required leading to a larger gas pressure in the main chamber and in the divertor [17].

3. H-MODE DENSITY LIMIT EXPERIMENT IN THE JET TOKAMAK WITH ITER-LIKE WALL

3.1 H-MODE DENSITY LIMIT ON JET WITH THE ITER-LIKE WALL

High density high confinement-mode (H-mode) plasmas are the baseline scenario for operation of ITER in high fusion gain regimes ($Q_{DT} \geq 10$) with plasmas at a density of 85% of the Greenwald Density Limit (GDL) scaling [18] and high energy (~350MJ) [1]. A dedicated H-mode density limit experiments with the ILW have been performed at $B_T \approx 3.0$T, $I_p = 2.0$MA in discharges with an additional NBI-power of 8-10.5MW in high-triangularity magnetic equilibria similar to those used in the all-carbon machine experiments. Figure 7 shows the time evolution of a typical H-mode density limit discharge in JET with the tungsten divertor. Deuterium external gas fuelling into the inner leg of the divertor was used in this NBI-heated discharge to raise the plasma density. The BeII (527nm) fast emission signal in the outer divertor represents the ELMs behaviour during the density

ramp. Typically, gas fuelled, high density H mode discharge can be described by three main stages as shown in Fig.7: a Type I ELM phase, then a small ELM regime, followed by the L-mode phase with energy confinement deterioration. A similar behaviour has been observed in the C-machine [19]: when external gas fuelling is applied to these discharges, the frequency of Type I ELMs increases with some reduction of the energy confinement of the plasma. Further increase of the fuelling source is associated with a transition from type I to small ELMs ($n_e/n_{GDL} = 0.8$, confinement factor of $H_{98Y} = 0.8$) and to a further reduction of the plasma energy content, compared to the Type I ELM phase. The radiation losses tend to increase during the Type I phase with following saturation at constant level of $\gamma = P_{rad}/P_{heat} = 0.45$ during the small ELMs phase. Although the small ELMs are associated with strongly reduced power loads on plasma-facing components, the deterioration of the energy confinement makes this regime less attractive for the future reactors. If the fuelling is maintained, the energy confinement is continuously reduced and a back transition at t=55.6s from H to L-mode is observed. The H-mode density limit is typically defined as the maximum of ne that is reached at the H-L boundary. The maximum density achieved in this gas fuelled steady state ELMy H-mode is ~105% of the GDL at an energy confinement factor of $H_{98Y} = 0.7$ and a radiation fraction of $\gamma = P_{rad}/P_{heat} = 0.45$.

3.2 ROLE OF DETACHMENT IN H-MODE DENSITY LIMIT

High density discharges in JET with the ITER-like wall have been analysed with the objectives of establishing a mechanism for the H-mode density limit. Figure 8 shows the observations made in the divertor during the approach to the limit in the H-mode density limit discharge already presented in section 3.1. In addition to Fig.7, the central panels show measurements of the integrated ion current to the inner divertor as well as the local saturation current at the outer strike point. The lower envelope of the saturation currents indicates the roll-over into detachment in the outer divertor leg after the Type I to small ELMs transition. Also shown are the pedestal density nped and pedestal temperature Tped. The pedestal as well as the central averaged densities do not saturate at the transition from type I to small ELMs and the latter reaches its maxima during the small ELMs phase. At the same time, the density increase is accompanied by a cooling of both ion and electrons. As the pedestal becomes denser and cooler, the Type I ELM frequency increases, as shown in figure 8. Additionally, the figure shows the D_γ-emission (top row) and D_γ/D_α ratio (bottom row) in the divertor region at four different points in time. The local increase of D_γ/D_α ratio at the outer strike point indicates the partial detachment of the outer leg directly after Type I -> small ELMs transition. At 15s the detachment propagates into the SOL and the D_γ/D_α-ratio increases strongly in the SOL indicating a completely detached outer divertor. The density in the core and at the edge is rising even when the outer divertor is completely detached while the pedestal Tped stabilises after the outer divertor is fully detached. Thus, detachment itself does not trigger the H-L Transition and thus does not present the limit on plasma density. The pedestal Tped is saturated/stabilised for a long-time period and cannot be below the H-mode threshold.

Figure 9 shows the tomographic reconstructions of D_γ (left) and BeII-emission (right) in the divertor region just before the H-L transition. The radiation patterns of hydrogen emission lines as well as Be emission are located in the outer leg outside the LCFS without any indication of the MARFE formation. Thus, detachment and MARFE do not trigger the H-L Transition and this experimental evidence supports the view of the earlier observation on JT-60U with [20] that it is the plasma confinement which is ultimately responsible for the H-mode density limit.

The power conducted to the SOL and divertor influences strongly the detachment: a reduction of the input power will lead to the early and stronger detachment. Because the detachment itself does not trigger the H-L transition, the pulses with different heating powers (8.0MW and 10.5MW) should have the same density limit. Figure 10 shows time traces of the selected signals (n_e (core), n_e (edge), P_{NBI}, D_2 fuelling rate and radiation level) for two H-mode density limit discharges ($B_T = 2.9T$, $I_p = 2MA$) in JET-ILW and identical magnetic field configuration. The heating power has been reduced from the 10.5MW (Pulse No: 81833, $P_{heat} - P_{rad} = 7.2MW$) to 8MW (Pulse No: 81934, $P_{heat} - P_{rad} = 5.3MW$). The behaviour of the plasma core density and of the edge density is very similar, even the H-L back transition happens at the same point in time. The density limit (central averaged density) and the pedestal density approach the same values independently of the heating power thus confirming the statement that the detachment does not trigger itself the H-L back transition.

3.3 COMPARISON OF THE H-MODE HIGH DENSITY OPERATION IN C- AND FULLY METALLIC MACHINE

In Fig.11 two density limit pulses (Pulse No: 81933–beryllium/tungsten wall; Pulse No: 76292 –carbon wall) with ITER-like and Carbon wall are compared. Both plasmas (2.0MA/≈3.0T) were heated with ≈10MW NBI. Similarly to the L-mode experiments, the density limit was higher (+20%) when the experiment was performed in the fully metallic machine. In contrast to JET-ILW, the total radiated power in JET-CFC is always increased during the density rise until the H-L transition. On the other hand, the radiation power with the ILW tends to increase during the Type I phase with following saturation at constant level of $\gamma = P_{heat} - P_{rad} = 0.45$ during the small ELMs phase. In general, the radiation fraction is always higher in the JET-CFC than in the JET-ILW. To reach the density limit in the full metal machine, essentially larger puffing rates than for the C-based machine are required.

A model proposed in JET for the interpretation of the ELMy H-mode ne-Te operational diagram [21,22] assumes that the transition from type I to small ELMs (same as for Type III ELMs), observed at high density, corresponds to a transition from an ideal to a resistive mode. Fig.11 shows that the transition from Type I to small ELMs (or to Type III ELMs in the case of C-wall) is accompanied by an increase of the edge collisionality ν^*(neo) at the pedestal. The edge collisionality ν^*(neo) [23] approaches extremely high values (between 4 and 6) for the pulse with JET-ILW directly after Type I –small ELMs transition indicating a much denser and cooler pedestal than in the C-machine.

According to the model developed by Borrass et al. [24], the onset of the H-mode density limit is related to the plasma detachment at the divertor plates between ELMs. This model extends the treatment of the L-mode density limit to the high density H-mode operations. The H-mode density limits in earlier experiments on JET and ASDEX-U with Carbon walls demonstrate a good agreement between experiment and this model. H-mode density limit in the machine with the ILW shows larger values (>40%) than predicted by Borrass.

The electron temperature Te and electron density ne profiles at the outer mid-plane around the edge barrier during the different phases of the H-mode density limit pulses with C- as well Be/W wall were measured by the High Resolution Thomson Scattering (HRTS) system [25].

The profiles developments show completely different behaviours as shown in Fig.12. In contrast to the full metallic machine, during the gas fuelling in carbon environment the $<n_e>$ saturates while the n_{ped} increases monotonically up to the H-L transition. The n_e profile approaches the flattening with density rise and T_e decreases monotonically until H-L transition followed by a drop in T_e after H-L transition.

In the case of the JET-ILW, the n_e profile is flat even at Type I-Small ELMs transition. Practically ncore has the same values as nped during the entire phase of density rise. The n_e profile stays flat until H-L transition. The T_e profile shows the strong reduction after Type I to small ELMs transition, then saturates and does not change even after the H-L transition.

Figure 12 confirms the previous statement that the metallic machine has a much denser and cooler pedestal than the C-machine.

CONCLUSIONS

L-mode and H-mode density limit experiments with the ILW have been investigated in the recent experimental campaign. The plasma density was raised steadily to the density limit by gas fuelling into the inner leg of the divertor at constant input power. The plasma has been driven in low- and high-triangularity magnetic equilibria similar to those used in the carbon machine experiments.

The L-mode density limit is in most cases disruptive and the onset of a limit is related to plasma detachment from the divertor targets with following formation of X-point MARFEs. In all observed magnetic field configurations the density limit observed is higher in JET-ILW than in JET-CFC. To reach the density limit in the fully metallic machine, essentially larger puffing rates than for the C-based machine are required. The radiation fraction is higher in the JET-CFC than in the JET-ILW; it leads to a reduction of powers flowing across the separatrix into the scrape-off layer and consequently to earlier detachment for the machine with C-wall. The ITER-like wall configuration demonstrates stable operation with a completely detached divertor or even with a stable X-point MARFE. Due to the much longer lifetime of the X-point MARFE in the JET-ILW than in the carbon environment, there is an excellent opportunity for the realization of a feedback control for stabilization of the operation domain under fully detached divertor conditions.

Whereas the density limit in L-mode JET plasmas with C-wall is generally disruptive, the extended

operation range with the ILW in high triangularity configuration can lead to a prompt transition to a mode with a stable "completely detached divertor" or even with a stable X-point MARFE and a disruption is not inevitable.

In contrary to the well-known "heating power independent" Greenwald limit, the L mode densities limit increases moderately with rising heating power independently of the wall material.

In H-mode, the rise in plasma density is accompanied by a degradation in energy confinement for fully metallic as well as for C-wall machines. The metallic machine operates with a much denser and cooler pedestal than the C-machine. The H-L transition constitutes an effective undisruptive density limit (the H mode density limit) for an H-mode plasma. Detachment itself does not trigger the H-L transition and thus does not present a limit on plasma density. The corresponding H mode studies show that before an H mode quenches into an L mode the maximum achievable density is practically independent of the heating power.

ACKNOWLEDGEMENT

This work, supported by the European Communities under the contract of Association between EURATOM and FZJ, was carried out within the framework of the European Fusion Development Agreement. The views and opinions expressed herein do not necessarily reflect those of the European Commission. Some of us obtained support from GA CR grant GA P205/10/2055 and the MSMT grant #LG11018 is acknowledged.

REFERENCES

[1]. Progress in the ITER Physics Basis, Edd., Nuclear Fusion **47** (2007) S1 sqq.
[2]. G.J. van Rooij, these Proceedings
[3]. G.F. Matthews et al., Physica Scripts **T145** (2011) 014001.
[4]. S. I. Krasheninnikov, Physics of Plasmas **4** (1997) 1638.
[5]. S. Brezinsek et al. Journal of Nuclear Materials **390–391** (2009) 267–273
[6]. A. Loarte, Journal of Nuclear Materials **241-243** (1997) 118.
[7]. G.M. McCracken et al 1998 Nuclear Fusion **38** 619 doi:10.1088/0029-5515/38/4/311
[8]. A.Huber et al 2012, to be published in Review of Scientific Instruments.
[9]. G.H.Golub and C.F. Van Loan, John Hopkins University Press, Baltimore, 1983.
[10]. M.E. Fenstermacher et al., Review of Scientific Instruments **68** (1) (1997) 974.
[11]. A.Huber et al., J. Nucl. Mater. **313-316** (2003) 925.
[12]. A.G. Meigs et al., these Proceedings
[13]. A.Huber et al., Journal of Nuclear Materials **363-365** (2007) 365.
[14]. M.Groth et al., these Proceedings
[15]. S. Brezinsek et al., these Proceedings
[16]. W. Fundamenski et al., Journal of Nuclear Materials **337-339** (2005) 305.
[17]. V. Philipps et al., these Proceedings

[18]. M. Greenwald et al., Plasma Physics and Controlled Fusion **44** (2002) R27.
[19]. G. Saibene et al 1999 Nuclear Fusion **39** 1133 doi:10.1088/0029-5515/39/9/307
[20]. A.V. Chankin et al., Plasma Physics and Controlled **44** (2002) A399.
[21]. A.V. Chankin et al., Plasma Physics and Controlled **41** (1999) 913.
[22]. G. Saibene et al., Plasma Physics and Controlled **44** (2002) 1769.
[23]. A. Loarte et al., Plasma Physics and Controlled **45** (2003) 1549.
[24]. K. Borrass et al., Nuclear Fusion **44** (2004) 752.
[25]. R. Pasqualotto et al., Review of Scientific Instruments **75** (2004) 3891

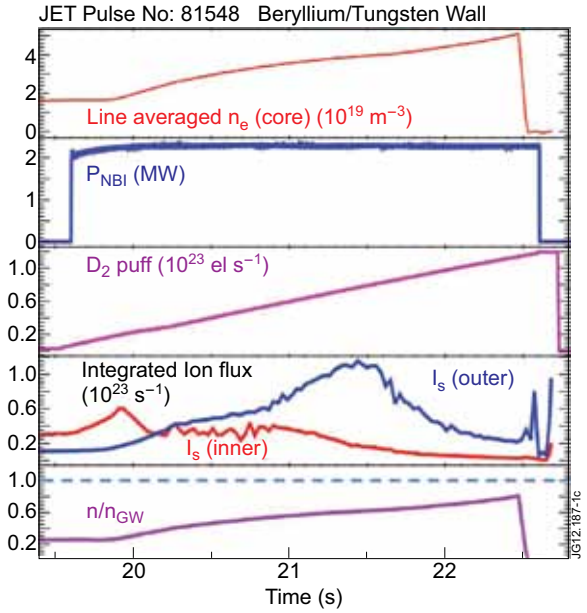

Figure 1: Selected plasma signals for a 1.7MA L-mode density limit discharge with the ILW

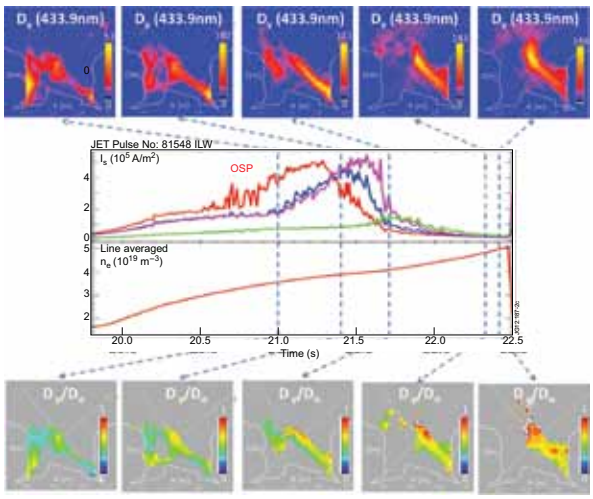

Figure 2: Tomographic reconstructions of Dγ-emission (top) and Dγ/Dα ratio (bottom) in the divertor region during the density ramp of the pulse discussed in figure1. The vertical dashed lines indicate the times at which the reconstructions are presented.

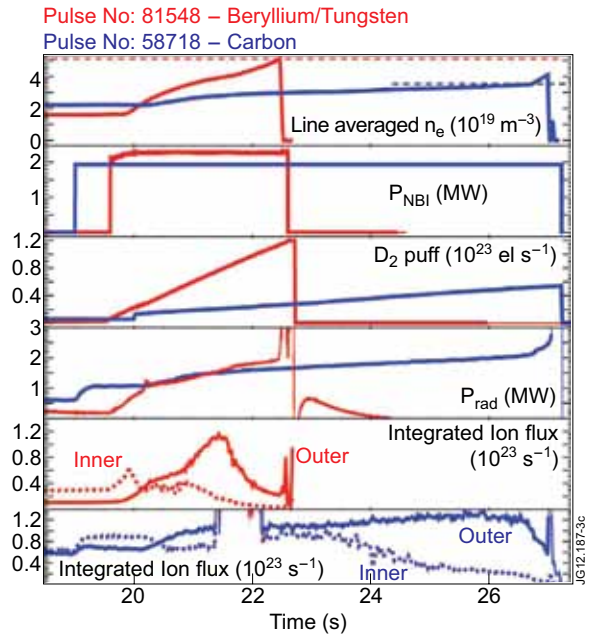

Figure 3: The ILW density limit discharge discussed in Figures 1 and 2 is directly compared with an identical case performed with the carbon wall.

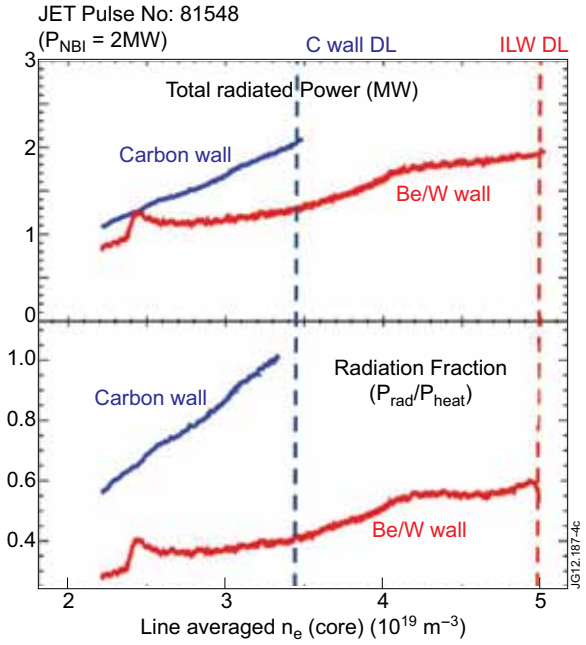

Figure 4: Total radiated power and radiation fraction versus <n_e> for JET-CFC and JET-ILW.

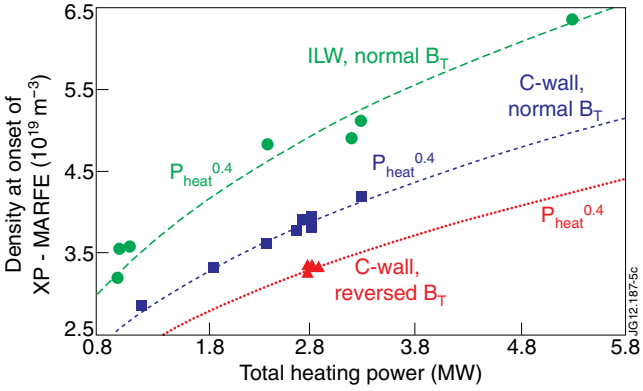

Figure 5: The line-averaged density at MARFE onset as a function of total heating power obtained in the JET-CFC and JET-ILW.

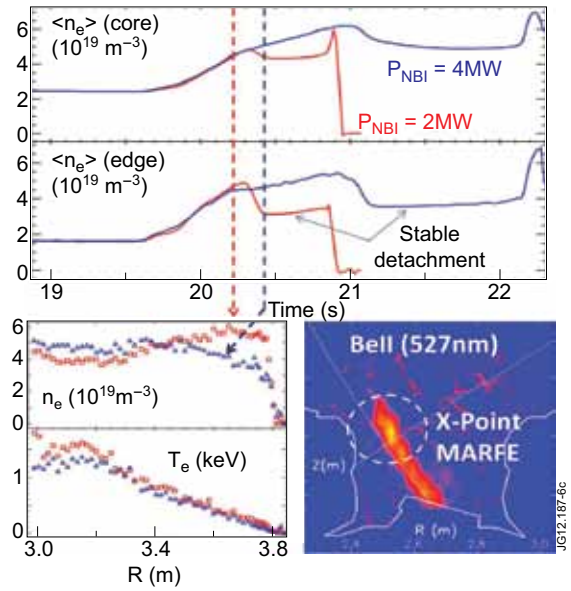

Figure 6: Time traces of the <n_e> in the core and at the edge of two L-mode discharges in JET with high triangularity configurations at P_{NBI} = 2MW and P_{NBI} =4MW.

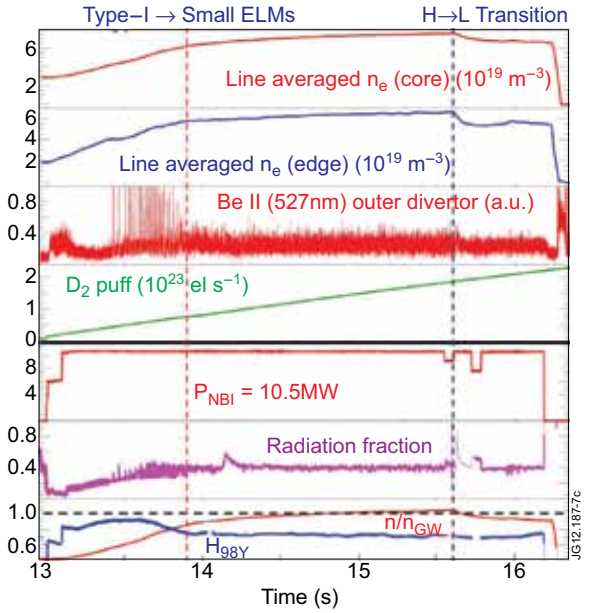

Figure 7: Time evolution of a typical H-mode density limit discharge in JET with the tungsten divertor.

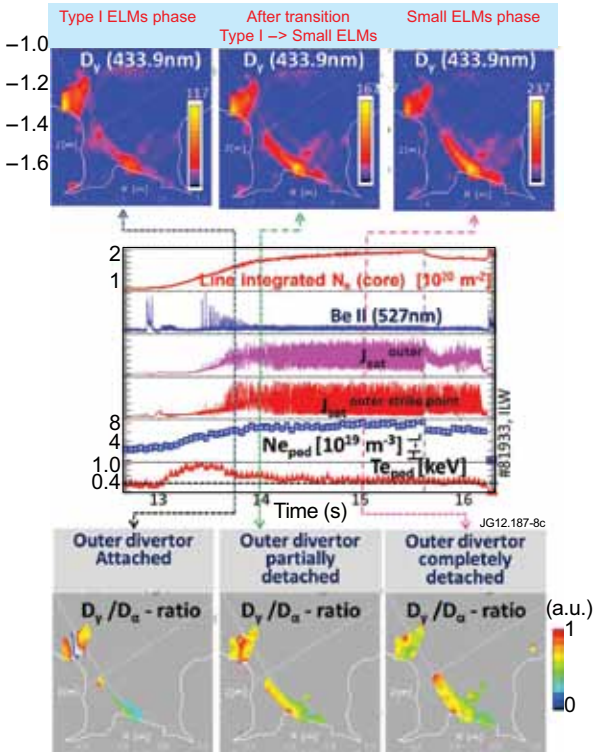

Figure 8: Tomographic reconstructions of D_γ-emission (top) and D_γ/D_α ratio (bottom) in the divertor region during three phases of the H-mode density limit discharge.

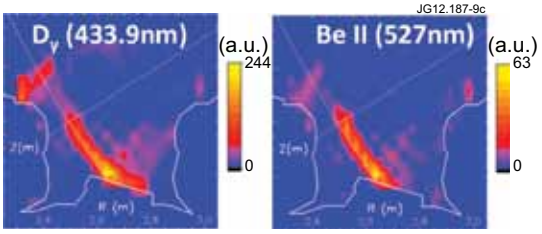

Figure 9: Tomographic reconstructions of D_γ (left) and BeII-emission (right) just before the H-L transition.

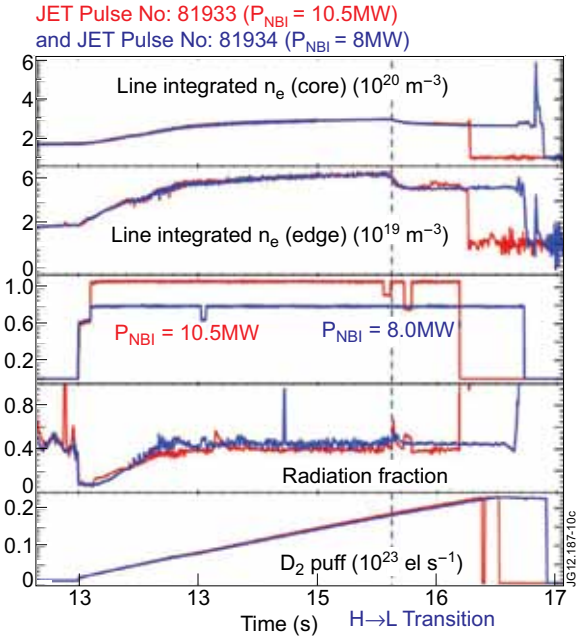

Figure 10: Time traces of the selected signals (n_e (core), n_e (edge), P_{NBI}, D_2 fuelling rate and radiation level) for two H-mode density limit discharges in JET-ILW and identical magnetic field configurations.

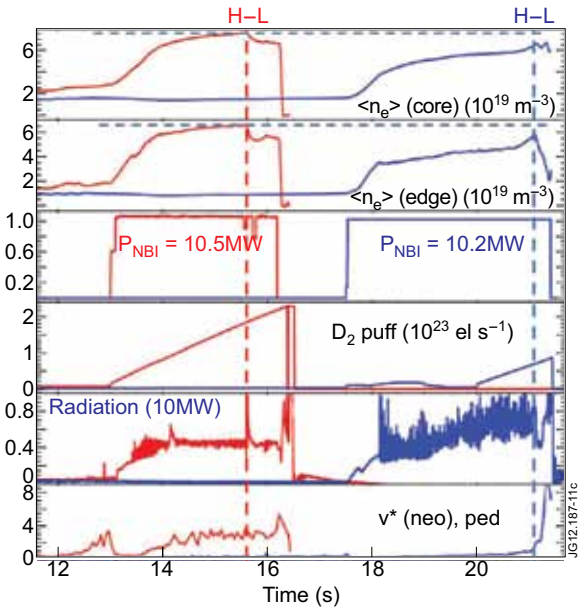

Figure 11: Comparison between two H-mode density limit pulses in JET-ILW and JET-CFC.

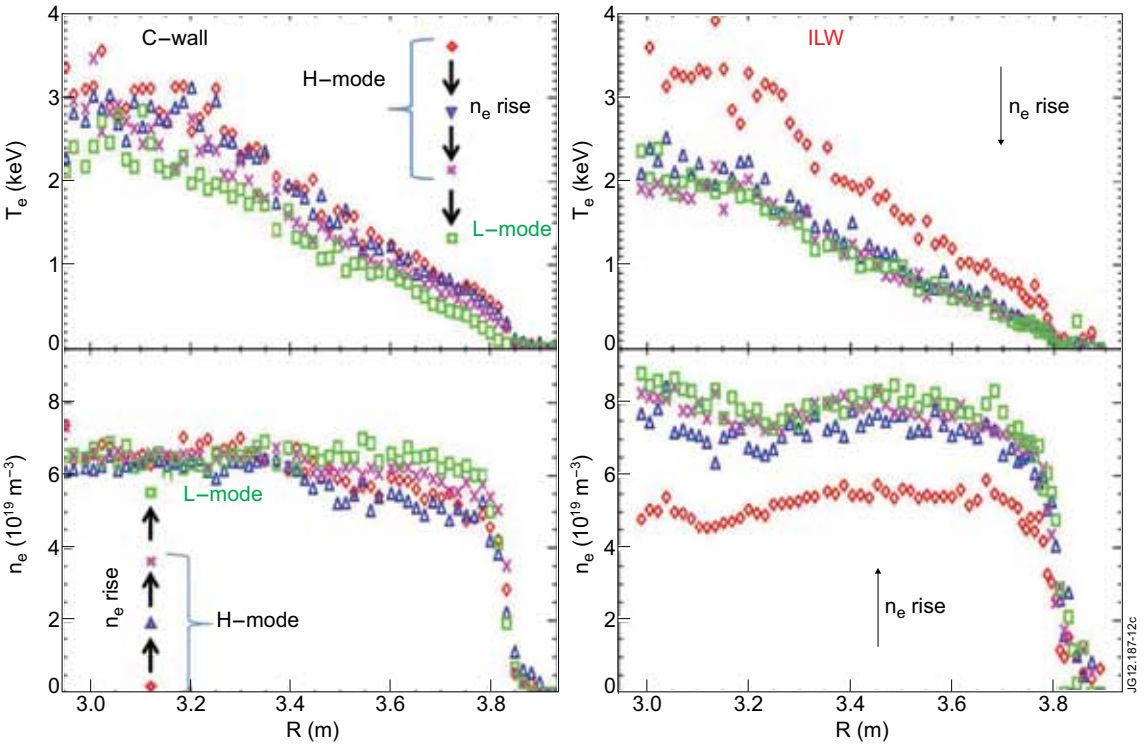

Figure 12: The Te and ne profiles during the different phases of the H-mode density limit pulses with C- as well with Be/W wall measured by the HRTS system.